



**HAL**  
open science

# Investigation of competitive COS and HCN hydrolysis reactions upon an industrial catalyst: Langmuir-Hinshelwood kinetics modeling

David Chiche, Jean-Marc Schweitzer

► **To cite this version:**

David Chiche, Jean-Marc Schweitzer. Investigation of competitive COS and HCN hydrolysis reactions upon an industrial catalyst: Langmuir-Hinshelwood kinetics modeling. *Applied Catalysis B: Environmental*, 2017, 205, pp.189-200. 10.1016/j.apcatb.2016.12.002 . hal-01518446

**HAL Id: hal-01518446**

**<https://hal.science/hal-01518446v1>**

Submitted on 4 May 2017

**HAL** is a multi-disciplinary open access archive for the deposit and dissemination of scientific research documents, whether they are published or not. The documents may come from teaching and research institutions in France or abroad, or from public or private research centers.

L'archive ouverte pluridisciplinaire **HAL**, est destinée au dépôt et à la diffusion de documents scientifiques de niveau recherche, publiés ou non, émanant des établissements d'enseignement et de recherche français ou étrangers, des laboratoires publics ou privés.

# Investigation of competitive COS and HCN hydrolysis reactions upon an industrial catalyst: Langmuir-Hinshelwood kinetics modeling

*David Chiche, \*<sup>a</sup> Jean-Marc Schweitzer<sup>a</sup>*

<sup>a</sup>IFP Energies nouvelles, Rond-point de l'échangeur de Solaize, BP 3, 69360 Solaize, France

\* To whom correspondence should be addressed. E-mail: [david.chiche@ifpen.fr](mailto:david.chiche@ifpen.fr)

## Abstract

Distinct and simultaneous COS and HCN hydrolysis reactions over an industrial TiO<sub>2</sub> based catalyst were extensively studied in this work in the scope of synthesis gas purification applications. 144 experiments were carried out, including 92 experiments that allowed to achieve partial conversion rates and showed reaction kinetics sensitivity to operating parameters. Significant crossed influences were evidenced between both COS and HCN hydrolysis reactions. The concomitant occurrence of both reactions showed to detrimentally affect each other upon COS and HCN conversion rates, and therefore upon kinetic rates. This was explained through a competitive adsorption of HCN and COS reactants upon catalyst surface active sites. Inhibition of catalytic activity by the presence of NH<sub>3</sub> and H<sub>2</sub>O (over a certain amount for the latter) was also evidenced and explained through competitive adsorption phenomena. For the operating conditions ranges explored, H<sub>2</sub>S and CO<sub>2</sub> had no sensitive impact on the kinetics of the COS and HCN hydrolysis reactions. However the moderate impact of CO<sub>2</sub> upon COS and HCN conversion rates might be explained by the large CO<sub>2</sub> excess compared to COS and HCN levels. A reaction model has been fully developed considering hydrodynamic, external mass transfer and intra particle diffusion limitations, and Langmuir-Hinshelwood reaction mechanisms for both COS and HCN hydrolysis reactions. Langmuir-Hinshelwood kinetic rate laws were indeed considered to account for the detrimental effect of gaseous species upon COS and HCN conversion kinetic rates, through competitive adsorption upon catalyst active sites of COS, HCN, H<sub>2</sub>O, and NH<sub>3</sub>. Collected kinetic data as a function of reactor size, gas residence time, temperature and

reactants partial pressures were used to validate and fit kinetic and adsorption constants. Very good agreement was achieved between experimental and calculated COS and HCN conversion rates from the model developed, that allowed complete validation of the Langmuir-Hinshelwood based modeling. The coupled hydrodynamic-reaction model also constitutes a complete industrial reactor model taking into account all the potential limitations, and can be used as a powerful predicting tool for industrial process design, *i.e.* fully usable for industrial process scale-up and optimization purposes.

## Graphical abstract

## Highlights

- Complete kinetic modeling of COS and HCN hydrolysis reactions have been performed.
- Full experimental study of T, GHSV, grain size, gas composition impact was achieved.
- HCN, COS, H<sub>2</sub>O and NH<sub>3</sub> competitive adsorptions have been evidenced and considered.
- The kinetic model has been implemented in a complete gas-solid reactor model.
- This model can be used as a powerful predicting tool for industrial process design.

## Keywords

Synthesis gas, purification, carbonyl sulfide, hydrogen cyanide, hydrolysis, kinetics modeling.

## Abbreviations

$A_p$ (m <sup>2</sup> )	Particle surface area
$\alpha_i$	Thermodynamic parameter
$\beta_i$	Thermodynamic parameter
T (K)	Temperature

$b_{COS}$ (bar <sup>-1</sup> )	COS adsorption constant
$b_{HCN}$ (bar <sup>-1</sup> )	HCN adsorption constant
$b_{NH_3}$ (bar <sup>-1</sup> )	NH <sub>3</sub> adsorption constant
$b_{H_2O}$ (bar <sup>-1</sup> )	H <sub>2</sub> O adsorption constant
$C_i^g$ (mol.m <sup>-3</sup> )	Gas concentration of compound $i$
$C_i^p$ (mol.m <sup>-3</sup> )	Particle concentration of compound $i$
$D_{ax}^g$ (m <sup>2</sup> .s <sup>-1</sup> )	Gas axial dispersion coefficient
$D_{eff,i}$ (m <sup>2</sup> .s <sup>-1</sup> )	Effective diffusion coefficient
$d_p$ (m)	particle diameter
$D_m$ (m <sup>2</sup> .s <sup>-1</sup> )	Molecular diffusion coefficient
$E_1$ (J.mol <sup>-1</sup> )	Activation energy of reaction 1
$E_2$ (J.mol <sup>-1</sup> )	Activation energy of reaction 2
$k_1$ (SI)	Kinetic constant of reaction 1
$k_2$ (SI)	Kinetic constant of reaction 2
$k_{gs}$ (m.s <sup>-1</sup> )	Gas-solid mass transfer coefficient
$K_{eq,i}$	$i^{th}$ thermodynamic constant
$L_c$ (m)	Particle characteristic length
$P_{COS}$ (bar)	COS partial pressure
$P_{CO_2}$ (bar)	CO <sub>2</sub> partial pressure
$P_{H_2S}$ (bar)	H <sub>2</sub> S partial pressure
$P_{HCN}$ (bar)	HCN partial pressure
$P_{CO}$ (bar)	CO partial pressure
$P_{H_2O}$ (bar)	H <sub>2</sub> O partial pressure
$P_t$ (bar)	Total pressure
Re	Reynolds number
$r_1$ (mol.s <sup>-1</sup> .kg <sup>-1</sup> )	Reaction rate of reaction 1
$r_2$ (mol.s <sup>-1</sup> .kg <sup>-1</sup> )	Reaction rate of reaction 2
R (J.mol <sup>-1</sup> .K <sup>-1</sup> )	Perfect gas constant

$r$ (m)	Radius coordinate
$R_p$ (m)	Particle radius
Sc	Schmidt number
Sh	Sherwood number
$V_p$ (m <sup>3</sup> )	Particle volume
$v_{sg}$ (m.s <sup>-1</sup> )	Superficial gas velocity
$z$ (m)	Reactor elevation
$\Delta H_{COS}$ (bar <sup>-1</sup> )	COS adsorption enthalpy
$\Delta H_{HCN}$ (bar <sup>-1</sup> )	HCN adsorption enthalpy
$\Delta H_{NH_3}$ (bar <sup>-1</sup> )	NH <sub>3</sub> adsorption enthalpy
$\Delta H_{H_2O}$ (bar <sup>-1</sup> )	H <sub>2</sub> O adsorption enthalpy
$\epsilon_g$	Gas holdup
$\epsilon_s$	Solid holdup
$\epsilon_p$	Particle porosity
$\delta$ (m)	Film thickness
$\mu_{i,j}$	Stoichiometric coefficient
$\rho_g$ (kg.m <sup>-3</sup> )	Gas density
$\rho_s$ (kg.m <sup>-3</sup> )	Solid density
$\tau$	Residence time
$\tau_p$	Particle tortuosity

# 1. Introduction

To protect the environment and preserve natural resources, a more diverse energy mix is essential, particularly in the transportation industry. As the only liquid fuels that can be used to supplement fossil based transportation fuels, biofuels play a major role in the diversification process.

Some research is currently focusing on the development of second-generation biofuels that can be made from non-edible, ligno-cellulosic materials derived from wood, straw, forest wastes, and dedicated crops [1,2]. By using the non-edible part of plants, second-generation biofuels are expected to enable to meet growing biofuel needs without competing with food production. In addition, they can use raw materials that are in abundant supply and deliver an interesting environmental performance. Second-generation biofuels can be produced from biochemical and thermochemical routes. Especially, as shown in Figure 1, thermochemical conversion consists in the gasification of carbonaceous feedstocks under partially oxidizing atmosphere into a synthesis gas (or syngas) composed of a CO-H<sub>2</sub> mixture [3]. After multiple gas conditioning steps aimed at reaching the required specifications (H<sub>2</sub>/CO ratio adjustment and CO<sub>2</sub> removal) [4,5], the syngas undergoes the Fischer-Tropsch reaction in order to produce synthetic liquid fuel [6–8]. However, synthesis gas also contains various impurities that must be removed in order to prevent Fischer-Tropsch catalyst poisoning [9–13].

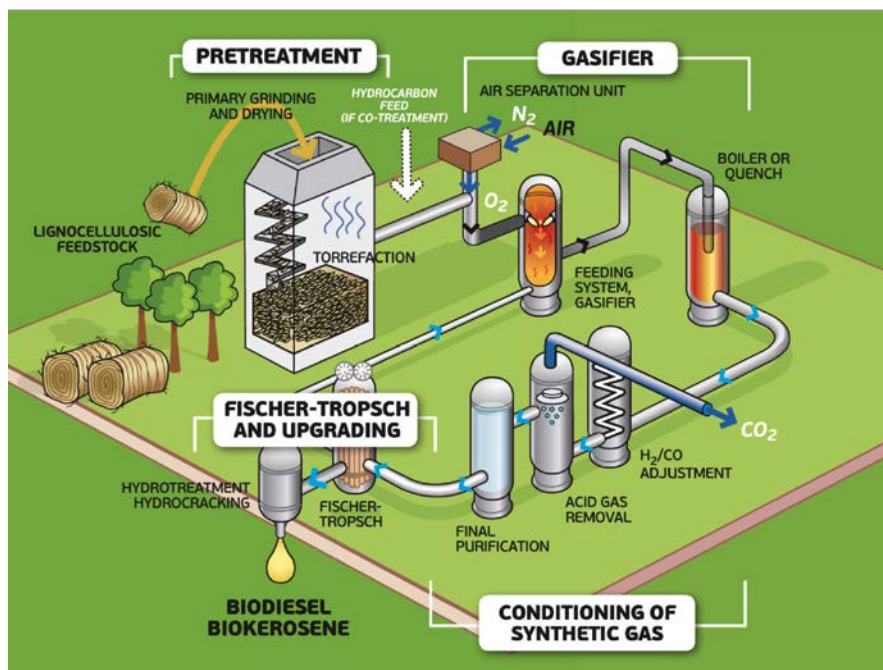


Figure 1. Schematic representation of the second-generation biofuels production chain from B-XTL thermochemical routes. (source IFPEN)

Integrated Gasification Combined Cycles (IGCC) power generation processes also constitutes more efficient and cleaner alternative technology for future energy production [14–16]. As for XTL based Fischer-Tropsch technology, this technology is also based on a first step of feed gasification into a synthesis gas. In IGCC power plants, the syngas is burnt into a gas turbine to produce electrical energy. Synthesis gas impurities such as H<sub>2</sub>S, COS and HCN, mixed to H<sub>2</sub>, are responsible for the corrosion of the industrial units [17], especially the combustion turbine blades used in IGCC processes.

Among the impurities present in synthesis gases, significant amounts of sulfur and nitrogen compounds are expected whatever the kind of feedstock (fossil or biomass), which are known to be severe poisons for Fischer-Tropsch catalysts [9,10,12,18], and responsible for the corrosion of industrial equipments [17].

Sulfur compounds should be present in the synthesis gas as H<sub>2</sub>S and COS, also depending on the gasification process operating conditions [3,11]. The presence of organic species such as mercaptans and thiophenic compounds in synthesis gases obtained from coal gasification is also reported [3]. It however may occur for gasification processes operating at low temperature (fixed or fluidized bed). In gasification processes operating at temperature higher than 1400°C such as entrained flow reactor, sulfur is only present in the synthesis gas as H<sub>2</sub>S and COS, and no organic sulfur compounds should be found downstream according to thermodynamic calculations. Biomass feedstocks generally have a much lower sulfur content than fossil feedstocks (coal, petcoke) [3,11,19,20]. Syngas H<sub>2</sub>S and COS contents may thus vary from hundreds to thousands of mol. ppm as a function of the feedstock.

Nitrogen species present in the feedstocks are converted into HCN and NH<sub>3</sub> in the gasification process. According to literature, the NH<sub>3</sub>/HCN ratio depends on many parameters [21–24], such as the nature of feedstocks (that may contain nitrogen compounds with different speciation), operating conditions of the gasification process such as pressure and temperature, gasification process technology (fixed bed, fluidized bed, entrained flow reactor). Nitrogen feedstock contents may vary from 0.1 to 3.3 mass.% [11,25–27], which affect accordingly the resulting nitrogen syngas contents after the gasification step [28]. In the gasification process, HCN formation is predominant from aromatic nitrogen compounds found in fossil feedstocks, whereas combustion of aminoacids and other nitrogen species usually present in biomass predominantly leads to the formation of NH<sub>3</sub> [3,11,22]. Syngas HCN contents may vary from a few mol. ppm to hundreds of mol. ppm, and NH<sub>3</sub> contents from a few mol. ppm to 14000 mol. ppm [3,11]. Other nitrogen compounds might also be present in synthesis gases such as

isocyanic acid HNCO, and nitrogen oxides NO<sub>x</sub>, also depending on the gasification operating conditions and technology [3,11].

Among existing purification technologies for COS and HCN removal [13,29], catalytic processes attract a great deal of interest. Indeed, both COS and HCN impurities can undergo hydrolysis reactions that are thermodynamically highly favored at low temperature. COS and HCN hydrolysis reactions can respectively be written as follows:



Catalysts are however required to improve both reactions kinetics. Regarding COS hydrolysis, most studied catalysts in the literature are metal oxides such as TiO<sub>2</sub>, Al<sub>2</sub>O<sub>3</sub>, ZnO and ZrO<sub>2</sub> [13,30–32]. Especially, catalyst activity seems to be related to catalyst surface basicity [33,34]. Alumina and TiO<sub>2</sub> supported catalysts, such as those used as catalysts in Claus processes, are also used for the COS conversion into H<sub>2</sub>S. Considering the activation energy, gamma alumina materials might be more active than TiO<sub>2</sub> materials [33,35], and should thus favor COS hydrolysis from lower temperature ( $T < 200^\circ\text{C}$ ). However, experimental observations evidence water inhibition on gamma alumina materials, occurring through a competitive adsorption on catalyst surfaces which results in a reduction of catalytic activity. As low water contents usually result in an increase of COS conversion, water inhibition effect is reported to occur above a certain H<sub>2</sub>O partial pressure, which also depends on COS partial pressure and temperature [32,36,37]. These effects have also been observed on other catalysts such as titania materials. For example, this has been reported in a comparative study on commercial catalysts based on alumina (Kaiser-201, Kaiser Aluminum and Chemicals) and titania (CRS 31, Axens) [35]. Alumina materials, which exhibit relatively high hydrophilic properties, seem to be more affected by catalytic inhibition by water than TiO<sub>2</sub> based materials. Therefore, under operating conditions close to industrial conditions, TiO<sub>2</sub> based catalysts seem to be more active than alumina catalysts. Temperature increase results in a diminution of catalytic inhibition to water, as this both favors kinetic rate increase and water desorption. More generally, catalytic inhibition is attributed to competitive adsorption with COS, that may hinder its conversion [32,36]. Such phenomena are also very likely to occur with reaction products (CO<sub>2</sub> and H<sub>2</sub>S) and other gas compounds that may be adsorbed on catalyst surface [38].

In synthesis gas applications, concomitant COS and HCN removal through hydrolysis process is possible, as catalysts for HCN hydrolysis are reported to be very similar to those used for



COS hydrolysis [30]. However, once again a competition between each hydrolysis reaction is likely to occur, through competitive adsorption of reactive species on catalysts surface. For each of these reactions, no reaction modeling taking into account any competitive adsorptions has been so far proposed in the literature, while extensive competitive adsorptions phenomena were proven to occur according to experimental data from literature [30,32]. Some kinetics modeling attempts were carried out using an Eley-Rideal model for single COS hydrolysis reaction, assuming COS hydrolysis through interaction of gaseous COS with adsorbed H<sub>2</sub>O [35,36]. In the latter, COS conversion through an intermediate adsorbed specie was not considered, in spite of evidences reported for the formation of intermediate surface hydrogeno-thiocarbonate specie [33,38,39].

In this article, we propose COS and HCN hydrolysis reactions modeling, considering for each reaction competitive adsorptions that may result from both reactants and products adsorption, as evidenced in the literature. The model will consider Langmuir-Hinshelwood mechanisms for each reaction, consistent with reported experimental observations [30,32], but never applied for kinetics interpretation and modeling. Both Langmuir-Hinshelwood rate laws proposed for COS and HCN hydrolysis reactions will also consider competitive adsorptions resulting from the simultaneity of both reactions. This kinetic model will be implemented in a complete gas-solid reactor model taking into account all transfer and transport limitations in order to predict industrial performances. Adsorptions of all the reactive species proven to affect reactions kinetics have been taken into account, *i.e.* COS, H<sub>2</sub>O, CO<sub>2</sub>, H<sub>2</sub>S, HCN, NH<sub>3</sub>. In this research, kinetic measurements for COS and HCN hydrolysis have been performed using an industrial TiO<sub>2</sub> based catalyst. Experiments were carried out under controlled conditions using lab scale fixed bed reactors.

## 2. Material and methods

Kinetic measurements were performed using a batch of an industrial TiO<sub>2</sub> based catalyst, on both uncrushed and crushed catalysts. Uncrushed catalyst is composed of 3 mm length extruded particles. Crushed catalyst particles were obtained after 0,5-1 mm sieving.

Experiments were carried out under controlled conditions using lab scale fixed bed reactors. A schematic representation of the experimental set-up is reported on Figure 2. This equipment can be divided in three sections, as represented in Figure 2:

1. A feed preparation zone where the different gas are mixed to build the feed gas. COS, CO<sub>2</sub>, He and H<sub>2</sub>S are supplied from gas tanks with specific gas compositions

provided by Air Liquide. A helium and water mixture is prepared using a water saturator set-up where an helium flow bubbles in water heated at a controlled temperature. This controlled water saturated helium flow is mixed to the mixture of dry COS-H<sub>2</sub>S-CO<sub>2</sub>-He gas to reach the desired water content.

2. A reaction zone, which basically consists in a cylindrical fixed bed reactor filled with the COS hydrolysis catalyst and heated at the desired temperature.

3. An analytic set-up to analyze and quantify the reactions products through on line mass spectrometry gas analyzer. Initial COS gas contents and COS gas contents downstream the hydrolysis reaction zone are measured to determine COS conversion rates as a function of the operating conditions.

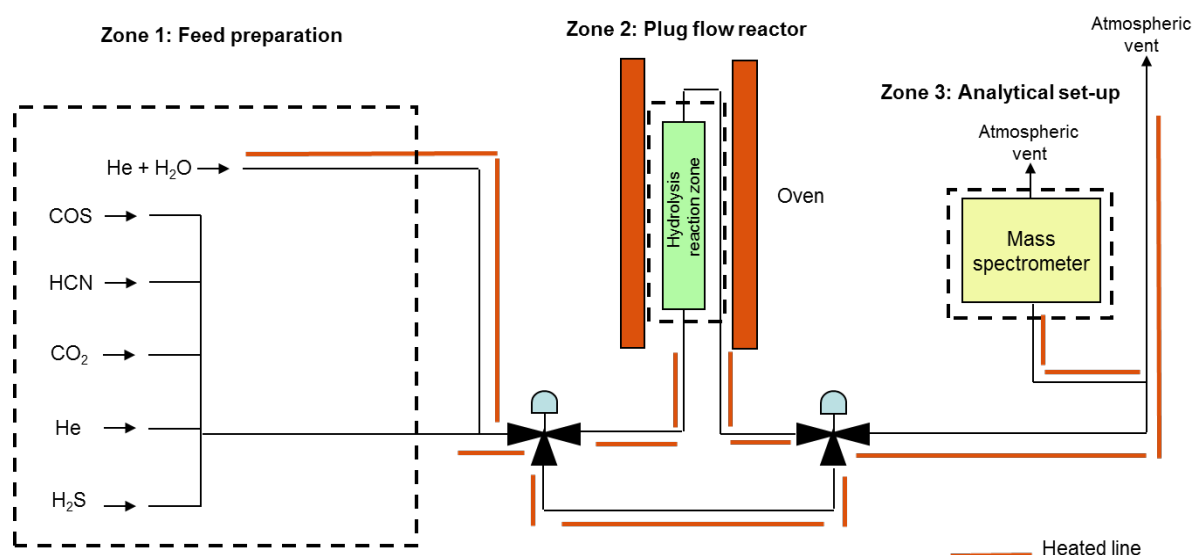


**Figure 2. Schematic representation of the experimental set-up used for kinetic measurements.**

Various reactor sizes were used, whose dimensions are reported on Table 1.

**Table 1. Reactors dimensions and filling.**

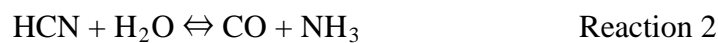
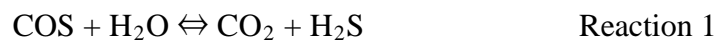
	Reactor #1	Reactor #2
Ø	2 cm	4 cm
h	7 cm	16 cm
V	22 mL	201 mL
Catalyst shaping	uncrushed	uncrushed
Catalyst weight	22 g	184 g

### 3. Theory and calculations

#### 3.1 Hydrolysis reactions kinetics and thermodynamics

A reaction model has been developed, based on a kinetic model validated with experiments obtained in a lab scale fixed bed reactor. First of all, the lab scale reactor is described taking into account all the limitations (external mass transfer and intra particle diffusion) in order to catch the so-called intrinsic kinetic parameters for COS and HCN hydrolysis reactions. Then, the following kinetic model has been implemented in a complete reactor model taking into account all the potential limitations.

As mentioned previously, COS and HCN can react with water according to the following reactions:



Both reactions are reversible. Thermodynamic equilibrium constants depend on the temperature as shown in Equation 1. Table 2 gives the corresponding thermodynamic parameters for the equilibrium constants.

$$\ln(K_{eq,i}) = \frac{\alpha_i}{T_{(K)}} + \beta_i \quad \text{Equation 1}$$

with  $i$  the reaction number (1 or 2).

**Table 2. HCN and COS hydrolysis reactions equilibrium constants.**

	$\alpha_i$	$\beta_i$	References
Reaction 1	3796.1	-0.5053	IFPEN experimental data
Reaction 2	6208.4	-0.5799	Fact sage data <a href="http://www.crct.polymtl.ca/fact/">http://www.crct.polymtl.ca/fact/</a>

For both reactions, a Langmuir-Hinshelwood reaction mechanism was considered to account for potential co-adsorption of gaseous species on catalyst surface active sites. Kinetic rate expressions for Reaction 1 and Reaction 2 are given respectively by Equation 2 and Equation 3:

$$r_{1(\text{mol/s/kg cat})} = k_1 \cdot e^{-\frac{E_1}{RT}} \cdot \frac{\left( P_{\text{COS}} \cdot P_{\text{H}_2\text{O}} - \frac{P_{\text{H}_2\text{S}} \cdot P_{\text{CO}_2}}{K_{eq,1}} \right)}{\left( 1 + \sum_i b_i e^{-\frac{\Delta H_i}{RT}} P_i \right)^2} \quad \text{Equation 2}$$

$$r_{2(\text{mol/s/kg cat})} = k_2 \cdot e^{-\frac{E_2}{RT}} \cdot \frac{\left( P_{\text{HCN}} \cdot P_{\text{H}_2\text{O}} - \frac{P_{\text{NH}_3} \cdot P_{\text{CO}}}{K_{eq,2}} \right)}{\left( 1 + \sum_i b_i e^{-\frac{\Delta H_i}{RT}} P_i \right)^2} \quad \text{Equation 3}$$

where  $i$  stands for each  $i$  gaseous compound.

Kinetic parameters for both reactions were estimated from lab scale experiments.

### 3.2 Reactor modeling

The lab scale fixed bed reactor device has been modeled to study COS and HCN hydrolyses reactions kinetics. A reactor model was developed considering a two-phase (gas-solid) fixed bed system operating under isothermal conditions, due to the low amount of reactants encountered. Indeed, heat transfers have been neglected, as COS and HCN gas contents remain very low, both for the lab scale experiments performed and most industrial cases ( $\ll 1\%$  v).

Different catalyst shapes can be used, cylinders or spheres, respectively accounting for experiments using uncrushed or crushed catalyst particles.

Material balances are written for each compound at different scales: in the gas flow, in the external mass transfer film around the catalyst particle, and inside the catalyst porous network. For the gas flow, a dispersed plug flow model was used in order to take into account potential back-mixing effect. Following Equation 4 gives the corresponding transient gas material balance:

$$\varepsilon_g \cdot \frac{\partial C_i^g}{\partial t} = D_{ax}^g \cdot \frac{\partial}{\partial z} \left( \varepsilon_g \cdot \frac{\partial C_i^g}{\partial z} \right) - \frac{\partial (v_{sg} \cdot C_i^g)}{\partial z} - k_{gs} \cdot \frac{\varepsilon_s}{L_c} \cdot (C_i^g - C_i^s) \quad \text{Equation 4}$$

Gas axial dispersion coefficient was estimated using the Gunn correlation [40] (Equation 5).

$$D_{ax}^g = \frac{v_{sg} / \varepsilon_g \cdot d_p}{\text{Pe}_a} \quad \text{Equation 5}$$

$$\text{with } \frac{1}{\text{Pe}_a} = X \cdot (1 - \phi)^2 + X^2 \cdot \phi \cdot (1 - \phi)^3 \cdot \left[ e^{\left( \frac{-1}{X \cdot \phi \cdot (1 - \phi)} \right)} - 1 \right] + \frac{\varepsilon_g}{\tau_p \cdot \text{Re} \cdot \text{Sc}}$$

$$\text{and } X = \frac{\text{Re} \cdot \text{Sc}}{21.13 \cdot \varepsilon_g}, \quad \text{Re} = \frac{\rho_g \cdot v_{sg} \cdot d_p}{\mu_g}, \quad \text{Sc} = \frac{\mu_g}{\rho_g \cdot D_m}$$

$$\phi = 0.17 + 0.33 \cdot e^{-\frac{24}{\text{Re}}}, \quad \tau = 1.4 \quad \text{for sphere}$$

$$\phi = 0.17 + 0.29 \cdot e^{-\frac{24}{\text{Re}}} \quad \tau = 1.93 \quad \text{for cylinder}$$

The material balance in the external film is given by Equation 6:

$$\delta \cdot \frac{\partial C_i^s}{\partial t} = k_{gs} \cdot (C_i^g - C_i^s) - D_{eff,i} \cdot \frac{\partial C_i^p}{\partial r} \Big|_{r=R_p} \quad \text{Equation 6}$$

with  $\delta = \frac{D_m}{k_{gs}}$  (film thickness) and  $L_c = \frac{V_p}{A_p}$  (characteristic length of the catalyst).

The mass transfer coefficient  $k_{gs,i}$  for each specie  $i$  is given by the Yoshida correlation [41], which takes into account the gas flow pattern around the particle (Equation 7).

$$\begin{aligned} \text{Sh} &= 0.983 \cdot \text{Re}^{0.59} \cdot \text{Sc}^{1/3} & \text{if } \text{Re} > 190 \\ \text{Sh} &= 1.66 \cdot \text{Re}^{0.49} \cdot \text{Sc}^{1/3} & \text{if } \text{Re} < 190 \end{aligned} \quad \text{Equation 7}$$

$$\text{with } \text{Sh} = \frac{k_{gs,i} \cdot d_p}{D_{m,i}}, \quad \text{Re} = \frac{\rho_g \cdot v_{sg} \cdot d_p}{\mu_g}, \quad \text{Sc} = \frac{\mu_g}{\rho_g \cdot D_{m,i}}.$$

Gas material balances should respect the equation of state  $\sum_i C_i^g = \frac{P_t}{R \cdot T}$  (perfect gas law assumption). Then, after summing all the gas equations and introducing the equation of state, the corresponding equation for the gas velocity is obtained (Equation 8):

$$\frac{\partial(v_{sg} \cdot P_t)}{\partial z} = D_{ax}^g \cdot \frac{\partial}{\partial z} \left( \varepsilon_g \cdot \frac{\partial P_t}{\partial z} \right) - R \cdot T \cdot \sum_i k_{gs,i} \cdot \frac{\varepsilon_s}{L_c} \cdot (C_i^g - C_i^s) \quad \text{Equation 8}$$

Particle material balances (Equations 9 and 10) are written for two particle shapes, cylinders and spheres, respectively accounting for uncrushed and crushed catalyst particles.

Spherical particle modeling:

$$\varepsilon_p \cdot \frac{\partial C_i^p}{\partial t} = \frac{D_{eff,i}}{r^2} \cdot \frac{\partial \left( r^2 \cdot \frac{\partial C_i^p}{\partial r} \right)}{\partial r} + \sum_j \mu_{i,j} \cdot r_j \cdot \rho_s \quad \text{Equation 9}$$

Cylindrical particle modeling:

$$\varepsilon_p \cdot \frac{\partial C_i^p}{\partial t} = \frac{D_{eff,i}}{r} \cdot \frac{\partial \left( r \cdot \frac{\partial C_i^p}{\partial r} \right)}{\partial r} + \sum_j \mu_{ij} \cdot r_j \cdot \rho_s \quad \text{Equation 10}$$

with  $\varepsilon_p$  particle porosity.

The effective diffusion coefficient is a function of the molecular diffusion coefficient of each compound, and of catalyst porosity and tortuosity (Equation 11):

$$D_{eff,i} = \frac{D_{m,i} \cdot \varepsilon_p}{\tau_p} \quad \text{Equation 11}$$

where  $\tau_p$  stands for catalyst tortuosity ( $2 < \tau_p < 5$ ), and  $\varepsilon_p$  catalyst porosity.

Effect of pressure and temperature on the molecular diffusion coefficient has been taken into account. Calculations of gas molecular diffusion have been carried out from Equation 12, as given by *Fuller et al.* [42]:

$$D_{iB} = \frac{1.43 \cdot 10^{-3} \cdot T^{1.75}}{P_t \cdot M_{iB}^{1/2} \cdot \left[ (\Sigma_v)_i^{1/3} + (\Sigma_v)_B^{1/3} \right]^2} \quad \text{with} \quad M_{iB} = \frac{2}{\frac{1}{M_i} + \frac{1}{M_B}} \quad \text{Equation 12}$$

Binary diffusion coefficient of compound  $i$  in a matrix  $B$ , which has been considered as equivalent to CH<sub>4</sub> one (intermediate molecular weight between H<sub>2</sub> and CO).

Reactor pressure drop is calculated using the Ergun relation [43] (Equation 13) or the Handley relation [44] (Equation 14) according to the gas flow regime.

$$\frac{dP}{dz} = \frac{150}{d_p^2} \cdot \frac{\varepsilon_s^2}{(1-\varepsilon_s)^3} \cdot \mu_g \cdot v_{sg} + \frac{1.75}{d_p} \cdot \frac{\varepsilon_s}{(1-\varepsilon_s)^3} \cdot \rho_g \cdot v_{sg}^2 \quad 0 < \text{Re}/\varepsilon_s < 1000 \quad \text{Equation 13}$$

$$\frac{dP}{dz} = \frac{368}{d_p^2} \cdot \frac{\varepsilon_s^2}{(1-\varepsilon_s)^3} \cdot \mu_g \cdot v_{sg} + \frac{1.24}{d_p} \cdot \frac{\varepsilon_s}{(1-\varepsilon_s)^3} \cdot \rho_g \cdot v_{sg}^2 \quad 1000 < \text{Re}/\varepsilon_s < 5000 \quad \text{Equation 14}$$

### 3.3 Numerical resolution

A spatial discretization of the partial derivative equations was performed using an upwind finite differences scheme for the convection terms, and a centered finite differences scheme for the diffusion or dispersion terms. For time integration, the LSODE solver was used based on a predictor-corrector algorithm [45]. An excel interface coupled with Matlab (for 3D visualization) was developed.

### 3.4 Model parameters optimization

Adsorption and kinetic parameters have been estimated using a Levenberg-Marquardt optimizing method [46]. This approach is based on a controlled Newton-Gauss numerical method. A statistical analysis of the optimized parameters is performed and a corresponding confidence interval of 95% is given for each of them. It is a way to evaluate the statistical significance of a parameter and if the model and the experimental data set are able to sensitize

it. The correlation matrix coming from this statistical analysis allows to help to choose the right experimental data subset to discriminate effects of correlated parameters. A part of the experimental data set is used for parameter optimization (experiments with COS or HCN conversion < 80%) and another part is used for model validation.

## 4. Results and discussion

### 4.1 Experimental data

COS and HCN hydrolysis reactions over  $\text{TiO}_2$  based catalyst in fixed bed reactor configuration has been studied. The experiments performed are aimed at validating Langmuir-Hinshelwood type rate laws and determining the sensitivity of reactions kinetics to operating parameters, namely reactants gas contents, temperature, and residence time. Residence times have been set to reach partial COS and HCN conversions (lower than 80% in most cases) to be able to monitor conversion variations as a function of other operating parameters (gas composition and temperature). This allowed to identify critical operating parameters, and especially gas compounds that affect reactions kinetics.

COS and HCN conversion rates achieved as a function of operating parameters for each experiments are then used for the validation of kinetic rates laws expected (Langmuir-Hinshelwood) and kinetic parameters determination through the model developed.

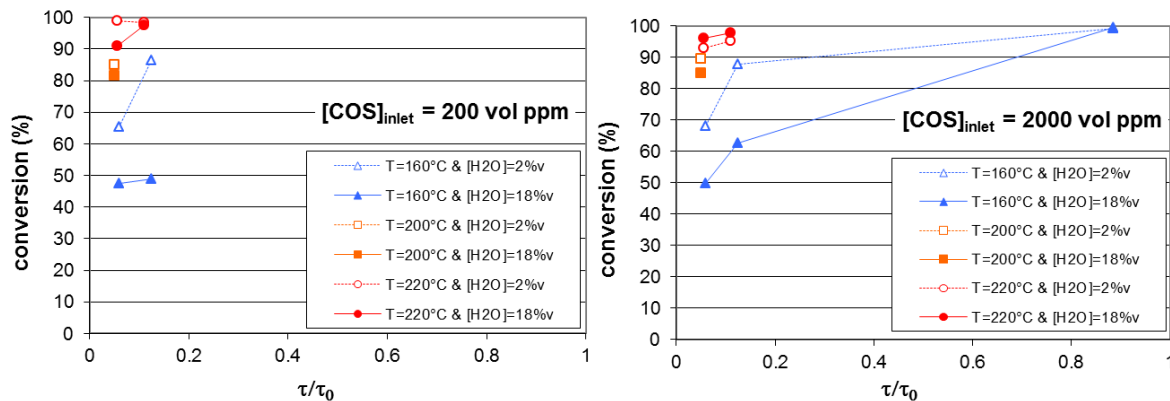
Influence of the following parameters on COS and HCN hydrolysis extent has been explored: reactants partial pressures (*i.e.* COS,  $\text{H}_2\text{O}$ ,  $\text{H}_2\text{S}$ ,  $\text{CO}_2$ , HCN,  $\text{NH}_3$ ), operating temperature, residence time (through variation of the gas hourly space velocity (GHSV)). Experiments have been performed in a synthesis gas matrix (in a  $\text{H}_2 - \text{CO} - \text{CO}_2$  mixture). Operating temperatures, pressure ranges, and gas composition explored are summarized in Table 3. Finally, 144 experiments have been performed, with 92 experiments for which partial COS and HCN conversion have been reached (lower than 80%). In the following, kinetic conversion rates will be expressed as a function of normalized residence time values, defined as the ratio of residence time  $\tau$  and a constant reference time value  $\tau_0$ .

**Table 3. Operating conditions ranges (T, P, gas composition).**

Laboratory operating conditions ranges	
T	60 – 280°C
P	1 – 20 bar
H <sub>2</sub>	25 – 57 vol. %
CO	22 – 55 vol. %
CO <sub>2</sub>	1.3 – 9.5 vol.%
H <sub>2</sub> O	0.5 – 18 vol. %
COS	0 – 2000 vol. ppm
H <sub>2</sub> S	0 – 20000 vol. ppm
HCN	0 – 1200 vol. ppm
NH <sub>3</sub>	0 – 6700 vol. ppm

### Effect of temperature

For each COS and HCN hydrolysis reaction, effect of temperature on conversion rate was explored. Figure 3 shows some of the results obtained for the hydrolysis of COS alone (no HCN nor NH<sub>3</sub>). It shows COS conversion rate, as a function of temperature and residence time, for various initial COS and water gas content. As expected, higher conversion rate are achieved with temperature increase. High conversion rate (> 98%) are obtained for temperature above 220°C and/or long residence times (normalized residence times values  $\tau/\tau_0 > 0.5$ ). Lower conversion rates are obtained for normalized residence times values  $\tau/\tau_0$  comprised between 0.05 and 0.25. These experiments achieved with low residence times can be used to explore COS hydrolysis reaction kinetics sensitivity to other operating parameters, by monitoring conversion rates variations.

**Figure 3. COS conversion rate as a function of temperature, water content and normalized residence time, for various COS inlet gas contents.**



Similar experiments were carried out on gas containing HCN and no COS nor H<sub>2</sub>S to evaluate the effect of temperature upon HCN hydrolysis over the TiO<sub>2</sub> based catalyst (results not shown). Concomitant COS and HCN hydrolysis experiments were also performed. Figure 4 shows some of the results obtained in the latter case.

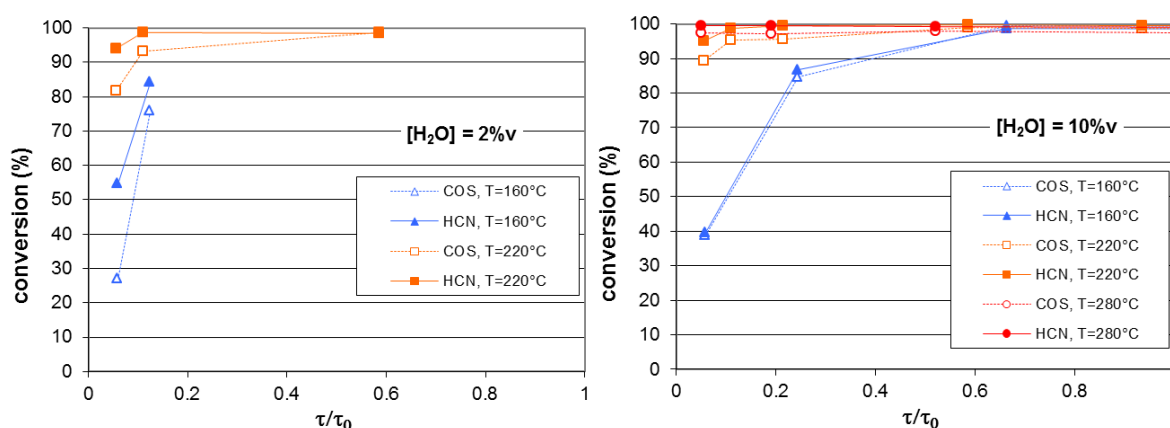


**Figure 4. COS and HCN conversion rates as a function of temperature and normalized residence time, for various H<sub>2</sub>O gas content, and for COS inlet gas content of 2000 vol ppm and HCN inlet gas content of 500 vol ppm.**

### Effect of H<sub>2</sub>O gas content

Although H<sub>2</sub>O is a reactant and allows COS and HCN hydrolysis, water molecules may compete with other reactants over adsorption on catalyst surface. Therefore, some experiments have been carried out to investigate possible inhibition of catalytic activity toward COS and HCN hydrolysis with increasing gas water content. Effect of temperature is also considered, as it may affect reactants adsorption. These experiments have been achieved for the study of separate COS hydrolysis (as shown in Figure 3), HCN hydrolysis (results not shown), and concomitant COS and HCN hydrolysis (as shown in Figure 4). Some of the results obtained are represented as a function of the initial H<sub>2</sub>O gas content in Figure 5. A decrease of both COS and HCN conversion rates is observed at 160°C with increasing H<sub>2</sub>O gas content. At 220°C, increase of H<sub>2</sub>O content does not affect conversion rates; one should however notice that due to the high conversion values at 220°C, the operating condition ranges explored for this latter set of experiments do not allow to highlight influence of water on reaction kinetics (lower residence times would be necessary here). Other consistent data (not shown) were acquired at intermediate temperatures (180°C and 200°C), and below 160°C

(60°C, 100°C, 120°C). These experiments clearly evidence an inhibition of catalytic activity below 180°C for the operating conditions ranges explored.

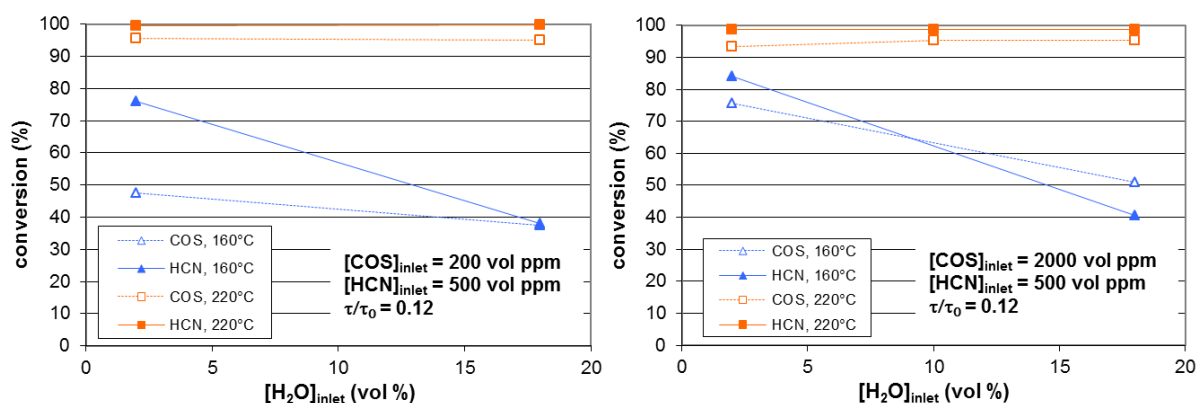


**Figure 5. COS and HCN conversion rates as a function of gas water content, for various operating temperatures, and inlet COS gas content. Residence time set is the same for each experimental point.**

### Effect of H<sub>2</sub>S and NH<sub>3</sub>

COS and HCN hydrolysis reaction products might also act as catalytic reaction inhibitor, through competitive adsorption on catalyst surface. The effect of H<sub>2</sub>S and NH<sub>3</sub> on COS and HCN hydrolysis reactions have been investigated. Figure 6 shows COS and HCN conversion rates as a function of H<sub>2</sub>S initial gas content. No effect is evidenced on COS and HCN conversion kinetics. As a consequence, H<sub>2</sub>S does not seem to compete toward HCN and COS adsorption on TiO<sub>2</sub> catalyst.

However, presence of NH<sub>3</sub> in the gas significantly affects HCN conversion. Figure 7 shows some of the results obtained in the case of HCN hydrolysis. NH<sub>3</sub> has therefore to be taken into account for reaction modeling.

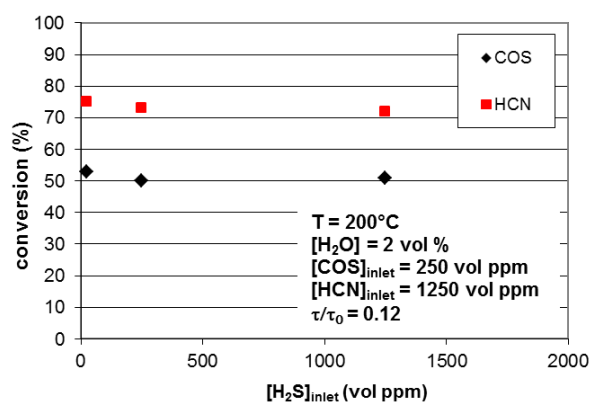


**Figure 6. COS and HCN conversion rates as a function of H<sub>2</sub>S inlet gas content. Residence time set is the same for each experimental point.**

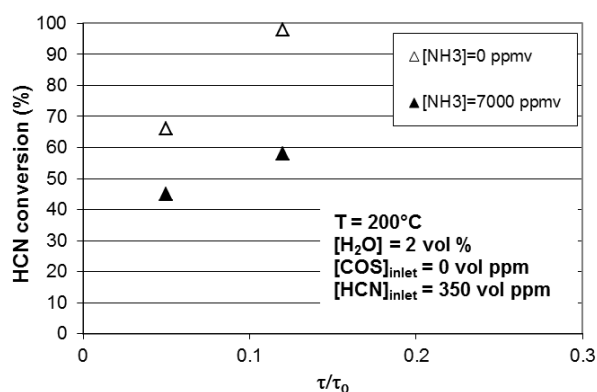


**Figure 7. HCN conversion rate as a function of NH<sub>3</sub> inlet gas content and normalized residence time.**

### Simultaneous HCN and COS hydrolysis reactions

As also shown previously, concomitant COS and HCN hydrolysis experiments were also carried out to explore how each reaction may affect each other. As previously discussed, according to literature [30–33,38], each COS and HCN hydrolysis reactions are expected to occur through adsorption of COS and HCN reactants and reaction products upon catalyst surface. As it was shown from previous experiments discussed, high H<sub>2</sub>O gas contents and NH<sub>3</sub> (for the operating ranges explored) were shown to affect kinetics, more likely through a competitive adsorption upon HCN and COS adsorption sites. This resulted in an inhibition of catalytic activity. No effect of H<sub>2</sub>S was evidenced in the operating conditions ranges explored (no competitive adsorption upon HCN and COS adsorption sites). Simultaneous COS and HCN hydrolysis experiments are therefore aimed at investigating whether simultaneous presence of HCN and COS species may affect each other upon their conversion kinetics. A full range of experiments have been carried out, showing significantly lower conversion rates for simultaneous COS and HCN hydrolysis, compared to conversion rates measured with COS or HCN alone in same conditions. Figure 8 shows some of results obtained for experiments with COS alone compared to same experiments with HCN added. These results clearly evidence a detrimental effect of the presence of HCN upon COS conversion. Catalytic inhibition effect could therefore result from the presence of HCN, and also from the presence of NH<sub>3</sub> formed through HCN hydrolysis. Similar results are obtained for HCN conversion, that evidence HCN conversion inhibition in the presence of COS (results not shown).

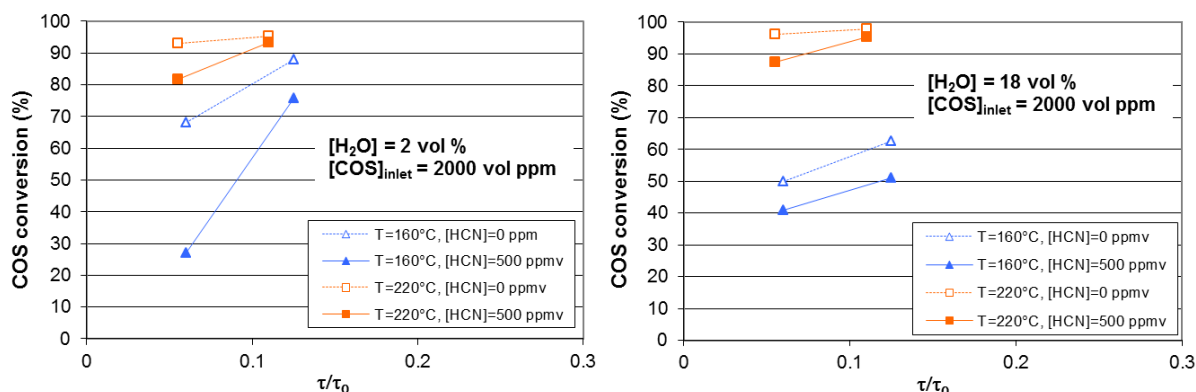


**Figure 8.** COS conversion rate as a function of HCN gas content and normalized residence time, for COS inlet gas content of 2000 vol ppm, and for various operating temperatures and H<sub>2</sub>O gas contents.

## 4.2 Hydrolysis reactions modeling

The experimental data (COS and HCN conversion rates as a function of operating conditions) were used to fit kinetic and adsorption constants of Langmuir-Hinshelwood kinetic rate laws for both COS and HCN hydrolysis reactions catalyzed by the industrial TiO<sub>2</sub> based catalyst used in this study, according to the procedure described in Section 3.

Kinetic constants  $k_i$ , and activation energies  $E_i$  for both reactions, as well as adsorption constants  $b_i$  and  $\Delta H_i$  for each gaseous compounds were estimated through kinetic model optimization from a first restricted set of experiments. This first set of 46 experiments was chosen from experiments showing most significant sensitivity toward operating parameters (temperature, and gas composition). This was performed in order to facilitate parameters optimization. The whole set of parameters was optimized simultaneously. Table 4 shows the optimized values of the activation energies, adsorption constants and enthalpies with the corresponding confidence intervals and  $t$ -values. Normalized kinetics constants and activation energies values of both COS and HCN hydrolysis reactions are reported, taking as a reference values obtained for the COS hydrolysis reaction  $k_1^\circ$  and  $E_1^\circ$ . This allows comparison between values obtained for both COS and HCN hydrolysis reactions.

**Table 4. Optimized parameters and statistical analysis.**

	<i>Kinetic parameters</i>				<i>Statistic test</i>
	Estimated values	Standard deviation	Lower limit	Upper limit	t-value
$k_1/k_1^\circ$	1.00	0.98	-1.07	2.85	0.9
$k_2/k_1^\circ$	2.41	5.11	-7.63	12.82	0.5
$E_1/E_1^\circ$	<b>1.00</b>	<b>0.18</b>	<b>0.63</b>	<b>1.37</b>	<b>5.4</b>
$E_2/E_1^\circ$	<b>1.11</b>	<b>0.33</b>	<b>0.44</b>	<b>1.78</b>	<b>3.3</b>
$b_{\text{COS}}$ (Pa <sup>-1</sup> )	4.49E-07	2.28E-06	-4.10E-06	5.00E-06	0.02
$b_{\text{HCN}}$ (Pa <sup>-1</sup> )	1.67E-03	1.39E-03	-1.11E-03	4.46E-03	1.2
$b_{\text{NH}_3}$ (Pa <sup>-1</sup> )	1.07E-11	3.24E-11	-5.42E-11	7.56E-11	0.3
$b_{\text{H}_2\text{O}}$ (Pa <sup>-1</sup> )	7.44E-07	6.19E-07	-4.93E-07	1.98E+06	1.2
$\Delta H_{\text{COS}}$ (J.mol <sup>-1</sup> )	-7054	35000	-77000	62900	-0.2
$\Delta H_{\text{HCN}}$ (J.mol <sup>-1</sup> )	-10829	3250	-17300	-4340	-3.3
$\Delta H_{\text{NH}_3}$ (J.mol <sup>-1</sup> )	-75314	11700	-98600	-52000	-6.5
$\Delta H_{\text{H}_2\text{O}}$ (J.mol <sup>-1</sup> )	-21646	2860	-27400	-15900	-7.6

Only five parameters (activation energies and adsorption enthalpies) are significant according to confidence intervals. The correlation matrix shows that pre-exponential factors  $b_i$  are strongly correlated with the corresponding energies  $\Delta H_i$  (Cf. Table 5). This correlation can be explained by the linear trend of exponential terms when the temperature range explored is too narrow. A wider experimental temperature range should be explored to de-correlate adsorption enthalpies from pre-exponential factors. Therefore, it was decided to set constant adsorption enthalpy values, in order to make sensitive the pre-exponential factors.

**Table 5. Correlation matrix for kinetic and adsorption constants determined from the model optimization.**

	$k_1$	$k_2$	$E_1$	$E_2$	$b_{\text{COS}}$	$b_{\text{HCN}}$	$b_{\text{NH}_3}$	$b_{\text{H}_2\text{O}}$	$\Delta H_{\text{COS}}$	$\Delta H_{\text{HCN}}$	$\Delta H_{\text{NH}_3}$	$\Delta H_{\text{H}_2\text{O}}$
$k_1$	<b>1.00</b>	0.01	<b>0.98</b>	0.02	-0.24	-0.03	0.11	-0.39	-0.05	0.00	0.06	-0.42
$k_2$	0.01	<b>1.00</b>	0.04	<b>0.99</b>	-0.33	0.47	-0.87	-0.10	-0.34	0.42	-0.83	-0.07
$E_1$	<b>0.98</b>	0.04	<b>1.00</b>	0.06	-0.25	-0.03	0.10	-0.45	-0.07	0.05	0.06	-0.44
$E_2$	0.02	<b>0.99</b>	0.06	<b>1.00</b>	-0.31	0.45	-0.85	-0.14	-0.33	0.43	-0.81	-0.09
$b_{\text{COS}}$	-0.24	-0.33	-0.25	-0.31	<b>1.00</b>	-0.32	0.13	0.06	<b>0.97</b>	-0.34	0.16	0.04
$b_{\text{HCN}}$	-0.03	0.47	-0.03	0.45	-0.32	<b>1.00</b>	-0.66	-0.02	-0.34	<b>0.96</b>	-0.67	-0.02
$b_{\text{NH}_3}$	0.11	-0.87	0.10	-0.85	0.13	-0.66	<b>1.00</b>	0.06	0.17	-0.59	<b>0.97</b>	0.04
$b_{\text{H}_2\text{O}}$	-0.39	-0.10	-0.45	-0.14	0.06	-0.02	0.06	<b>1.00</b>	0.11	-0.11	0.07	<b>0.98</b>
$\Delta H_{\text{COS}}$	-0.05	-0.34	-0.07	-0.33	<b>0.97</b>	-0.34	0.17	0.11	<b>1.00</b>	-0.37	0.19	0.08
$\Delta H_{\text{HCN}}$	0.00	0.42	0.05	0.43	-0.34	<b>0.96</b>	-0.59	-0.11	-0.37	<b>1.00</b>	-0.62	-0.07
$\Delta H_{\text{NH}_3}$	0.06	-0.83	0.06	-0.81	0.16	-0.67	<b>0.97</b>	0.07	0.19	-0.62	<b>1.00</b>	0.06
$\Delta H_{\text{H}_2\text{O}}$	-0.42	-0.07	-0.44	-0.09	0.04	-0.02	0.04	<b>0.98</b>	0.08	-0.07	0.06	<b>1.00</b>

Table 6 with  $t$ -values reported from the statistic test shows that most of the pre-exponential factors become significant ( $t$ -values  $\geq 2$ ) when energy values are fixed. This means that the experimental data set is able to sensitize the activities and the adsorptions of many species. Nevertheless, COS adsorption does not seem to have a significant impact, as  $t$ -values are close to 0 for COS adsorption parameters, and as  $b_{COS} \cdot \exp(-\Delta H_{COS}/RT)$  values can be neglected in comparison to other adsorption terms on the whole temperature range explored. This may result from a lack of information in the experimental data set used for the modeling. Another possibility is that adsorption of these compounds could be neglected as it would not significantly affect reactions kinetics. The latter would be in agreement with previous high temperature COS hydrolysis modeling through Eley-Rideal mechanism performed by *Tong et al.* on other  $TiO_2$  based catalyst [35]. Further experimental investigations should be carried out in order to discriminate between both hypotheses.

**Table 6. Statistical analysis of the parameters with adsorption enthalpy values set constant.**

	<i>Kinetic parameters</i>				<i>Statistic test</i>
	<b>Estimated values</b>	<b>Standard deviation</b>	<b>Lower limit</b>	<b>Upper limit</b>	<b>t-value</b>
$k_1/k_1^\circ$	1.00	0.33	0.23	1.54	2.7
$k_2/k_1^\circ$	2.41	0.81	0.97	4.21	3.2
$b_{COS}$ (Pa <sup>-1</sup> )	4.49E-07	2.31E-04	-4.61E-04	4.62E-04	0.002
$b_{HCN}$ (Pa <sup>-1</sup> )	1.67E-03	3.67E-04	9.38E-04	2.41E-03	4.6
$b_{NH_3}$ (Pa <sup>-1</sup> )	1.07E-11	5.58E-12	-4.49E-13	2.19E-11	1.9
$b_{H_2O}$ (Pa <sup>-1</sup> )	7.44E-07	1.39E-07	4.67E-07	1.02E-06	5.4

Kinetic constants values are compared to values reported for an Eley-Rideal modeling, and obtained for COS hydrolysis on another  $TiO_2$  based catalyst on temperature range of 270°C to 330°C [35]. Reported kinetic constants as a function of temperature are in the same order of magnitude (*Cf.* Table 7), even though temperature ranges explored for both studies and the catalysts used are different. No data were found regarding HCN hydrolysis on similar materials; kinetic constants can be found calculated on other materials (model materials  $Al_2O_3$  and  $TiO_2$ ) and with other formalism [30].

**Table 7. Comparison with COS hydrolysis kinetic constant as reported from *Tong et al.* for an Eley-Rideal modeling of data obtained on other TiO<sub>2</sub> based catalyst [35].**

T (°C)	270	300	330
Kinetics constants ratio $\frac{k \cdot K_3}{k_1 \cdot e^{-\frac{E_1}{RT}}}$	3.6	1.9	1.3

with  $k \cdot K_3$  the COS hydrolysis kinetic constant from Eley-Rideal model as reported by *Tong et al.* (*Tong et al.* notation), and  $k_1 \cdot e^{-\frac{E_1}{RT}}$  the COS hydrolysis kinetic constant from the Langmuir-Hinshelwood model as calculated in the present study.

Adsorption constants values obtained for HCN, NH<sub>3</sub>, H<sub>2</sub>O are therefore in agreement with a competition model for adsorption of these species towards catalyst active sites. Each specie compete towards adsorption on surface active sites, and may therefore interfere between each other for adsorption. As shown in experimental parts, the presence of NH<sub>3</sub> and H<sub>2</sub>O (over a certain amounts for the latter) results in inhibition of catalytic activity for both COS and HCN reactions.

Furthermore, as the experiments did not show any sensitivity of the presence of H<sub>2</sub>S, and of gaseous major compounds (H<sub>2</sub>, CO, CO<sub>2</sub>) upon hydrolysis reactions kinetics (for operating conditions ranges explored), adsorption constants for these species calculated from model optimization were logically equal to 0. General Langmuir-Hinshelwood kinetic rate laws given in Equation 2 and Equation 3 for both reactions can therefore be expressed according to the following:

$$r_{1(mol/s/kg\ cat)} = k_1 \cdot e^{-\frac{E_1}{RT}} \cdot \frac{\left( P_{COS} \cdot P_{H_2O} - \frac{P_{H_2S} \cdot P_{CO_2}}{K_{eq,1}} \right)}{\left( 1 + b_{HCN} e^{-\frac{\Delta H_{HCN}}{RT}} P_{HCN} + b_{H_2O} e^{-\frac{\Delta H_{H_2O}}{RT}} P_{H_2O} + b_{NH_3} e^{-\frac{\Delta H_{NH_3}}{RT}} P_{NH_3} \right)^2}$$

$$r_{2(mol/s/kg\ cat)} = k_2 \cdot e^{-\frac{E_2}{RT}} \cdot \frac{\left( P_{HCN} \cdot P_{H_2O} - \frac{P_{NH_3} \cdot P_{CO}}{K_{eq,2}} \right)}{\left( 1 + b_{HCN} e^{-\frac{\Delta H_{HCN}}{RT}} P_{HCN} + b_{H_2O} e^{-\frac{\Delta H_{H_2O}}{RT}} P_{H_2O} + b_{NH_3} e^{-\frac{\Delta H_{NH_3}}{RT}} P_{NH_3} \right)^2}$$

Parity diagram showing calculated COS and HCN conversions from model optimization as a function of related experimental conversions is represented in Figure 9. The results obtained for the first set of 46 experiments used for parameters optimization are only represented. This shows good agreement between experimental and calculated values.

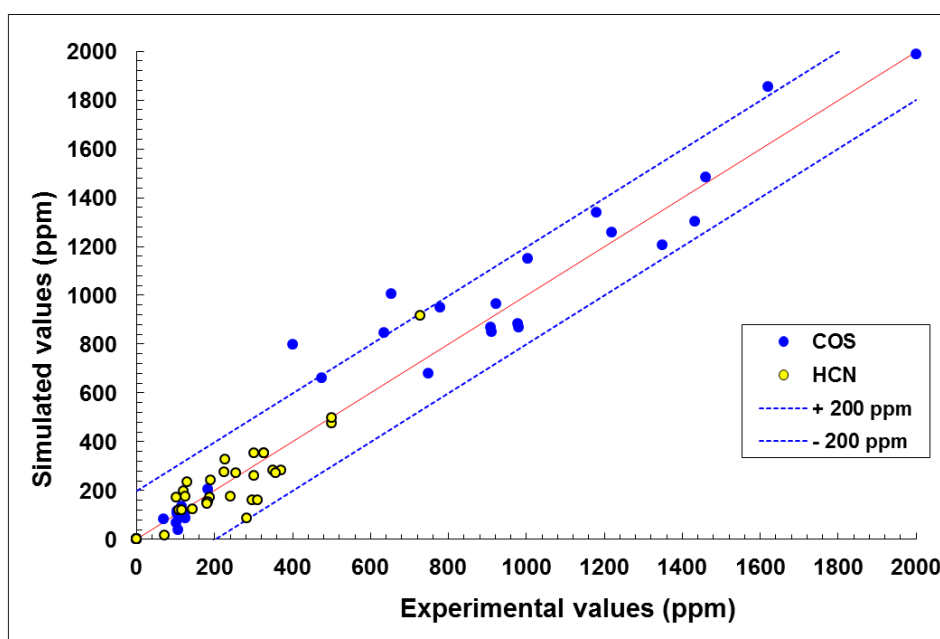


**Figure 9. Parity diagram giving calculated COS and HCN gas content from model optimization as a function of related experimental COS and HCN content after reaction. Results obtained for the first set of 46 experiments used for parameters optimization are only represented.**

Parity diagram showing calculated versus experimental conversions for the whole 92 experiments exhibiting partial COS and HCN conversions ( $< 80\%$ ) is represented in Figure 10. Some discrepancies are evidenced, some simulated values giving an overestimation of COS and HCN remaining contents compared to experimental values. Discrepancies seem to be higher for COS conversion than for HCN. This might be explained by the high amount of  $\text{CO}_2$  considered in gas matrix, and not taken into account for the experimental sensitivity study (as present in high concentration in synthesis gas applications). Indeed,  $\text{CO}_2$  may also compete with COS on similar adsorption sites [37,38].



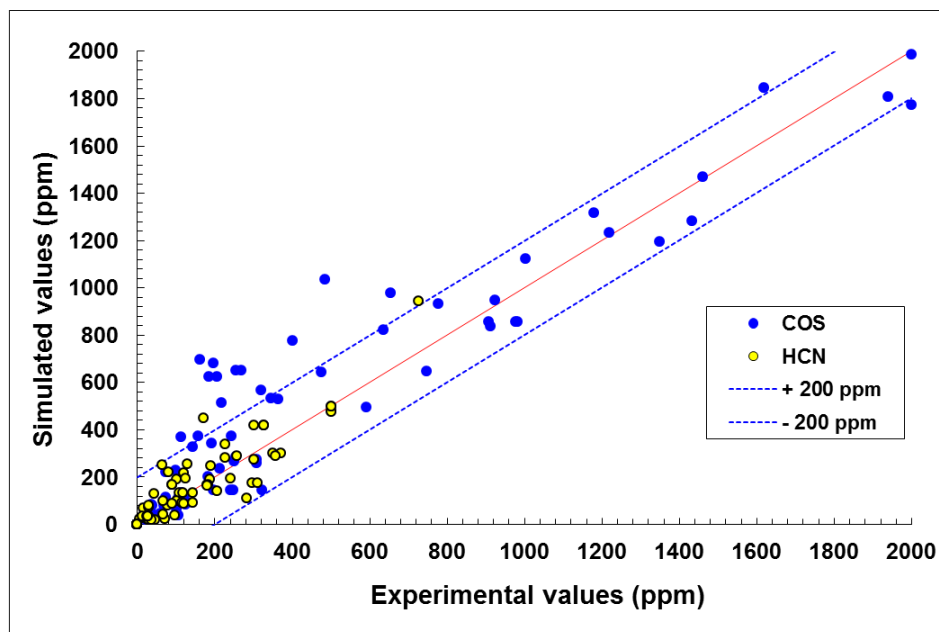


Figure 10. Parity diagram giving calculated COS and HCN gas content from model optimization as a function of related experimental COS and HCN content after reaction, for the whole 92 experiments (with conversions lower than 80%).

Significant transport limitations have been observed at the bed inlet due to the high reaction rates. Low transport limitations are observed at reactor outlet, due to lower COS and HCN gas content resulting from hydrolysis reactions along the reactor. COS and HCN intra particle concentrations profiles at different reactor elevations calculated from the reaction model are represented in Figure 11.

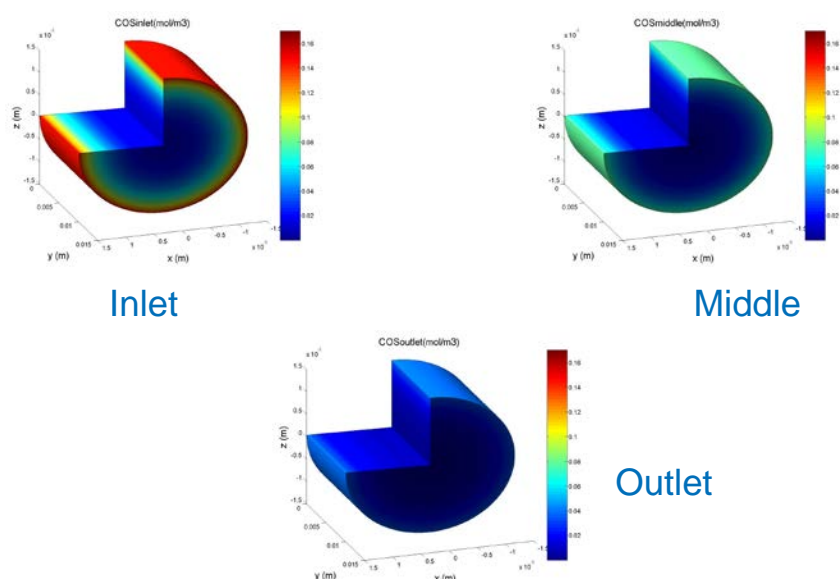


Figure 11. Particle COS concentration profiles at different axial positions in the reactor.

A data analysis can be performed from Thiele modulus calculations to further estimate the extent of macroporous diffusion limitations evidenced from the modeling. Thiele modulus calculations give an estimation of the limitations encountered, which are function of the relative importance of reaction kinetic towards mass transport [47]. The expression of Thiele modulus derived from *Rajadhyaksha et al.* in the case of Langmuir-Hinshelwood kinetics has been used [48]. Thiele modulus  $\phi$  is given by the following relation, as expressed using the article notation in the case of COS hydrolysis reaction:

$$\phi = \frac{1}{1 + b_{COS} \cdot e^{-\frac{\Delta H_{COS}}{RT}} \cdot P_{COS}} \cdot \sqrt{\frac{P_{COS}}{\ln\left(1 + b_{COS} \cdot e^{-\frac{\Delta H_{COS}}{RT}} \cdot P_{COS}\right)}} \cdot L_c \cdot \sqrt{\frac{k_1 \cdot e^{-\frac{E_1}{RT}} \cdot 1}{b_{H_2O} \cdot e^{-\frac{\Delta H_{H_2O}}{RT}} \cdot D_{COS}}}$$

with  $k_1$  the kinetic rate constant as calculated from the modeling for the COS hydrolysis reaction (*Cf.* Section 4.2),  $E_1$  activation energy for COS hydrolysis,  $b_{COS}$  and  $\Delta H_{COS}$  respectively the COS adsorption constant and enthalpy,  $D_{COS}$  the effective molecular diffusion coefficient of COS (calculated from the Fuller correlation [42], *Cf.* Equation 12),  $L_c$  the particle characteristic length defined as the ratio of particle volume  $V_p$  over particle external surface  $A_p$ .

Thiele modulus calculations for some operating conditions for lab scale experiments as a function of particle size (crushed *vs.* uncrushed particles) are given in Table 8. Thiele modulus values  $\phi > 1$  evidence mass transport limitations, whereas kinetics limitations are evidenced for  $\phi < 1$ . The calculations reported in Table 8 show for uncrushed particles that the higher the temperature, the higher the reaction kinetics along with induced mass transport limitations. Together with kinetics and 3D modeling of reactants and products gradients inside particles (Figure 11), this shows the occurrence of mass transport limitations inside catalyst porosity, due to significantly high catalyst activity for the COS hydrolysis reaction (high kinetic rate favored with increasing temperature). As a consequence, the extent of mass transport limitations will be also more pronounced with increasing particle size and/or pressure (the latter affecting molecular diffusivity). Same conclusions arise from the data analysis performed for the HCN hydrolysis reaction (not shown).

Interest for other shape of catalyst is therefore clearly evidenced, such as multilobe shape (trilobe), whose specific outer surface is increased and characteristic diameter decreased. Such shapes would contribute to enhance catalyst efficiency, taking advantage of the high catalytic

activity, and lowering the intra particle diffusional limitations resulting from the fast reactions kinetics.

**Table 8. Estimation of transport limitations from Thiele modulus calculations for some representative experimental conditions. Numerical application to the case of COS hydrolysis reaction.**

Mean particle diameter:	Lab-scale experiments			
	Uncrushed (cylindrical particle): $d_p = 3$ mm		Crushed (spherical particle): $d_p = 0.75$ mm	
	150°C	220°C	150°C	220°C
Thiele modulus $\phi$	1.07	2.64	0.18	0.44

## 5. Conclusions

COS and HCN hydrolysis reactions over an industrial  $\text{TiO}_2$  based catalyst were extensively studied in this work. 144 experiments were carried out, including 92 experiments that allowed to achieve partial conversion rates and showed reaction kinetics sensitivity to operating parameters. Significant crossed influences were evidenced between both COS and HCN hydrolysis reactions. The concomitant occurrence of both reactions showed to detrimentally affects each other upon COS and HCN conversion rates, and therefore upon kinetic rates. This was explained through a competitive adsorption of HCN and COS upon catalyst surface active sites. Inhibition of catalytic activity by the presence of  $\text{NH}_3$  and  $\text{H}_2\text{O}$  (over a certain amount for the latter) was also evidenced. For the operating conditions ranges explored,  $\text{H}_2\text{S}$  and  $\text{CO}_2$  had no sensitive impact on the kinetics of the COS and HCN hydrolysis reactions. However the moderate impact of  $\text{CO}_2$  upon COS and HCN conversion rates might be explained by the large  $\text{CO}_2$  excess compared to COS and HCN levels. High amounts of  $\text{CO}_2$  were indeed considered for lab scale tests, as typical synthesis gas matrices were used. However, one should also expect detrimental effect of the presence of  $\text{CO}_2$  due to competitive adsorption towards catalytic active sites. For higher conversion rates, the presence of  $\text{H}_2\text{S}$  and  $\text{CO}_2$  may also decrease the conversion performances due to thermodynamic equilibrium limitations.

A full reaction model has been fully developed considering hydrodynamic, external mass transfer and intra particle diffusion limitations, and Langmuir-Hinshelwood reaction mechanisms for both COS and HCN hydrolysis reactions. Langmuir-Hinshelwood kinetic rate

laws were considered to account for the detrimental effect of gaseous species upon COS and HCN conversion kinetic rates, through competitive adsorption upon catalyst active sites of COS, HCN, H<sub>2</sub>O, and NH<sub>3</sub>. Collected kinetic data as a function of reactor size, gas residence time, temperature and reactants partial pressures were used to validate and fit kinetic and adsorption constants. Good agreement was achieved between experimental and calculated COS and HCN conversion rates from the model developed. This allowed to validate the Langmuir-Hinshelwood kinetic rate laws. Additional experimental work has to be carried out to evaluate more accurately adsorption contribution of COS and NH<sub>3</sub>. Moreover, a larger temperature range will be explored in order to de-correlate pre-exponential factors from corresponding adsorption enthalpies.

Langmuir-Hinshelwood kinetic rate laws included in the plug flow reactor model developed can be used as a powerful modeling tool for a better understanding of physical-chemical phenomena involved in both COS and HCN hydrolysis reactions upon an industrial TiO<sub>2</sub> based catalyst. This coupled hydrodynamic-reaction model also constitutes a complete industrial reactor model taking into account all the potential limitations, and can be used as a powerful predicting tool for industrial process design, *i.e.* fully usable for industrial process scale-up and optimization purposes.

Intra particle diffusional limitations were evidenced, resulting from fast reactions kinetics. Interest for other shape of catalyst is therefore clearly evidenced, such as multilobe shape (*e.g.* trilobe), which would contribute to enhance catalyst efficiency, taking advantage of the high catalytic activity, and lowering the intra particle diffusional limitations resulting from the fast reactions kinetics.

## Acknowledgments

The authors thank Jean-Pierre Reyt (IFPEN) for technical help on catalytic apparatus.

## References

References

- [1] A. Demirbas, Progress in Energy and Combustion Science 33 (2007) 1–18.
- [2] D. Ballerini, Biofuels - Meeting the energy and environmental challenges of the transportation sector, 2012.
- [3] C. Higman, M. van der Burgt, Gasification, 2009.

- [4] A. Kohl, R. Nielsen, *Gas Purification*, Elsevier, Houston, 1997.
- [5] C. Ratnasamy, J.P. Wagner, *Catalysis Reviews-Science and Engineering* 51 (2009) 325–440.
- [6] H. Schulz, *Applied Catalysis A: General* 186 (1999) 3–12.
- [7] Van der Laan, G. P., Beenackers, A. A. C. M., *Catalysis Reviews-Science and Engineering* 41 (1999) 255–318.
- [8] A. Steynberg, M. Dry (Eds.), *Studies in Surface Science and Catalysis*, Fischer-Tropsch Technology, Elsevier, 2004.
- [9] O. Borg, N. Hammer, B.C. Enger, R. Myrstad, Lindvag, O. A., Eri, S., T.H. Skagseth, E. Rytter, *Journal of Catalysis* 279 (2011) 163–173.
- [10] S.S. Pansare, J.D. Allison, *Applied Catalysis A: General* 387 (2010) 224–230.
- [11] W. Torres, S.S. Pansare, J.G. Goodwin, *Catalysis Reviews* 49 (2007) 407–456.
- [12] B.S. Turk, T. Merkel, A. Lopez-Ortiz, R.P. Gupta, J.W. Portzer, G. Kishman, B.D. Freeman, G.K. Fleming, *Novel technologies for gaseous contaminants control*, US Department of Energy, National Energy Technology Laboratory, 2001.
- [13] D. Chiche, C. Diverchy, A.C. Lucquin, F. Porcheron, F. Defoort, *Oil & Gas Science and Technology* 68 (2013) 707–723.
- [14] O. Shinada, A. Yamada, Y. Koyama, *Energy Conversion and Management* 43 (2006) 1221–1233.
- [15] D. Vallentin, *Energy Policy* 36 (2008) 3198–3211.
- [16] M.J. Prins, K.J. Ptasinski, Janssen, F. J. J. G., *Fuel Processing Technology* 86 (2005) 375–389.
- [17] E.M. Jallouli, J.P. Larpin, M. Lambertin, J.C. Colson, *Oxidation of Metals* 11 (1977) 335–354.
- [18] M.J.A. Tijmensen, A.P.C. Faaij, C.N. Hamelinck, van Hardeveld, M. R. N., *Biomass and Bioenergy* 23 (2002) 129–152.
- [19] M. Asadullah, T. Miyazawa, S.I. Ito, K. Kunimori, M. Yamada, K. Tomishige, *Applied Catalysis A: General* 267 (2004) 95–102.
- [20] A. Demirbas, *Energy Conversion and Management* 44 (2003) 1465–1479.
- [21] J. Leppälähti, *Fuel* 74 (1995) 1363–1368.
- [22] J. Leppälähti, T. Koljonen, *Fuel Processing Technology* 43 (1995) 1–45.
- [23] H. Orikasa, A. Tomita, *Energy & Fuels* 17 (2003) 1536–1540.
- [24] P. Dagaut, P. Glarborg, M.U. Alzueta, *Progress in Energy and Combustion Science* 34 (2008) 1–46.

- [25] R. Alvarez-Rodriguez, C. Clemente-Jul, J.A. Martin-Rubi, *Fuel* 86 (2007) 2081–2089.
- [26] F. Frandsen, K. Damjohansen, P. Rasmussen, *Progress in Energy and Combustion Science* 20 (1994) 115–138.
- [27] A. van der Drift, J. van Doorn, J.W. Vermeulen, *Biomass and Bioenergy* 20 (2001) 45–56.
- [28] J. Zhou, S.M. Masutani, D.M. Ishimura, S.Q. Turn, C.M. Kinoshita, *Industrial & Engineering Chemistry Research* 39 (2000) 626–634.
- [29] S. Watson, R. Kimmitt, R.B. Rhinesmith, *Oil & Gas Journal* 101 (2003) 66–73.
- [30] M. Huisman, *The hydrolysis of carbonyl sulfide, carbon disulfide and hydrogen cyanide on titania catalysts*, 1994.
- [31] P.D.N. Svoronos, T.J. Bruno, *Industrial & Engineering Chemistry Research* 41 (2002) 5321–5336.
- [32] Rhodes C., Riddel S. A., West J., Williams B. P., Hutchings G. J., *Catalysis Today* 59 (2000) 443–464.
- [33] Aboulayt A., Mauge F., Hoggan P. E., Lavalley J. C., *Catalysis Letters* 39 (1996) 213–218.
- [34] Haffad D., Kameswari U., Bettahar M. M., Chambellan A., Lavalley J. C., *Journal of Catalysis* 172 (1997) 85–92.
- [35] S. Tong, I.G. Dalla Lana, K.T. Chuang, *The Canadian Journal of Chemical Engineering* 71 (1993) 392–400.
- [36] R. Fiedorow, R. Léauté, I.G. Dalla Lana, *Journal of Catalysis* 85 (1984) 339–348.
- [37] West J., Williams B. P., Young N., Rhodes C., Hutchings G. J., *Catalysis Letters* 74 (2001) 111–114.
- [38] Hoggan P. E., Aboulayt A., Pieplu A., Nortier P., Lavalley J. C., *Journal of Catalysis* 149 (1994) 300–306.
- [39] B.P. Williams, N.C. Young, J. West, C. Rhodes, G.J. Hutchings, *Catalysis Today* 49 (1999) 99–104.
- [40] D.J. Gunn, *Chemical Engineering Science* 42 (1987) 363–373.
- [41] F. Yoshida, T. Koyanagi, *Aiche Journal* 8 (1962) 309–316.
- [42] E.N. Fuller, J.C. Giddings, *Journal of Chromatographic Science* 3 (1965) 222–227.
- [43] S. Ergun, A.A. Orning, *Chemical Engineering Progress* 48 (1952) 89–94.
- [44] D. Handley, P.J. Heggs, *Transactions of the Institution of Chemical Engineers and the Chemical Engineer* 46 (1968) 251–264.

- [45] K. Radhakrishnan, A.C. Hindmarsh, NASA Reference Publication 1327 Lawrence Livermore National Laboratory Report UCRL-ID-113855 (1993).
- [46] D.W. Marquardt, Journal of the Society for Industrial and Applied Mathematics 11 (1963) 431–441.
- [47] Thiele, E. W., Industrial & Engineering Chemistry 31 (1939) 916–920.
- [48] R.A. Rajadhyaksha, K. Vasudeva, L.K. Doraiswamy, Journal of Catalysis 41 (1976) 61–71.